Journal of Solid State Chemistry 182 (2009) 122–128

Contents lists available at ScienceDirect

Journal of Solid State Chemistry

journal homepage: www.elsevier.com/locate/jssc

Structure and magnetic properties of rare-earth chromium germanides $RECr_xGe_2$ (RE = Sm, Gd–Er)

Haiying Bie, Andriy V. Tkachuk, Arthur Mar *

Department of Chemistry, University of Alberta, Edmonton, Alberta, Canada T6G 2G2

ARTICLE INFO

Article history:
Received 17 August 2008
Received in revised form
7 October 2008
Accepted 13 October 2008
Available online 22 October 2008

Keywords:
Rare earth
Germanide
Crystal structure
Magnetic properties

ABSTRACT

The ternary rare-earth chromium germanides $RECr_xGe_2$ (RE = Sm, Gd–Er) have been obtained by reactions of the elements, either in the presence of tin or indium flux, or through arc-melting followed by annealing at 800 °C. The homogeneity range is limited to $0.25 \leqslant x \leqslant 0.50$ for $DyCr_xGe_2$. Single-crystal and powder X-ray diffraction studies on the $RECr_{0.3}Ge_2$ members revealed that they adopt the $CeNiSi_2$-type structure (space group $Cmcm$, $Z = 4$, $a = 4.1939(5)$–$4.016(2)$ Å, $b = 16.291(2)$–$15.6579(6)$ Å, $c = 4.0598(5)$–$3.9876(2)$ Å in the progression for RE = Sm to Er), which can be considered to be built up by stuffing transition-metal atoms into the square pyramidal sites of a "$REGe_2$" host with the $ZrSi_2$-type structure. (The existence of $YbCr_{0.3}Ge_2$ is also implicated.) Only the average structure was determined here, because unusually short Cr–Ge distances imply the development of a superstructure involving distortions of the square Ge net. Magnetic measurements on $RECr_{0.3}Ge_2$ (RE = Gd–Er) indicated that antiferromagnetic ordering sets in below T_N (ranging from 3 to 17 K), with additional transitions observed at lower temperatures for the Tb and Dy members.

1. Introduction

Ternary rare-earth transition-metal germanides RE–M–Ge represent a well-investigated class of intermetallics exhibiting a wide range of structures and physical properties [1,2]. However, those systems containing an early transition metal are still not as well understood as those containing a late transition metal. In particular, reports in the RE–Cr–Ge systems have been restricted to isolated compounds ($Sc_2Cr_4Ge_5$ [3], $Sc_7Cr_{4+x}Ge_{10-x}$ [3,4], $ScCrGe_2$ [3,5], La_5CrGe_3 [6], $Nd_2Cr_9Ge_8$ [7], and $Sm_{117}Cr_{52}Ge_{112}$ [8]) and only two well-defined series ($RECr_6Ge_6$ (RE = Sc, Tb–Er) [3,9,10] and $RECrGe_3$ (RE = La–Nd, Sm) [11]), the latter having been identified recently by us. One series that has been missing to date is the set of $CeNiSi_2$-type phases that are adopted by a large number of silicides, germanides, and stannides, REM_xTt_2 (M = Mn, Fe, Co, Ni, Cu, Ru, Rh, Pd, Re, Ir, Pt; Tt = Si, Ge, Sn (collectively, the "tetrels")) [12,13]. Most of these phases are nonstoichiometric, with the transition-metal content x generally increasing on proceeding to a heavier transition metal or to a lighter tetrel. Surprisingly, detailed single-crystal structure studies have been scarce, and only recently has a modulated superstructure been implicated for $TbFe_{0.25}Ge_2$ [14]. Much of the interest on these REM_xTt_2 phases has focused on their varied magnetic properties, which depend systematically on the component elements [15].

Continuing our studies of the RE–Cr–Ge systems, we report here the new nonstoichiometric ternary germanides $RECr_xGe_2$, which form for the later RE elements (RE = Sm, Gd–Er). Some members could be successfully grown as single crystals through flux methods to permit structural investigations to determine the level of Cr deficiency in the $CeNiSi_2$-type structure adopted. Magnetic measurements were also performed for those members that could be prepared as phase-pure samples.

2. Experimental

2.1. Synthesis

Starting materials were RE pieces (99.9%, Hefa), Cr powder (99.8%, Alfa-Aesar), and Ge powder (99.999%, Cerac). Products were characterized by powder X-ray diffraction (on an Inel powder diffractometer equipped with a CPS 120 detector) and energy-dispersive X-ray (EDX) analysis (on a Hitachi S-2700 electron microscope).

Single crystals of $SmCr_xGe_2$ were first identified as byproducts in the synthesis of $SmCrGe_3$. The elements were loaded in the ratio Sm:Cr:Ge = 1:1:3 (total weight: 0.3 g) in the presence of 0.5 g Sn, which acts as a flux, into an inner alumina crucible

* Corresponding author. Fax: +1 780 492 8231.
E-mail address: arthur.mar@ualberta.ca (A. Mar).

0022-4596/$ - see front matter © 2008 Elsevier Inc. All rights reserved.
doi:10.1016/j.jssc.2008.10.013

jacketed by an outer fused-silica tube. The tube was heated up to 850 °C over 2 days, kept at that temperature for 4 days, and slowly cooled to 500 °C at a rate of 3 °C h^{-1}, at which point the liquid tin flux was centrifuged. Single crystals of $GdCr_xGe_2$ and $DyCr_xGe_2$ were prepared in a similar manner, through a reaction of *RE*:Cr:Ge = 1:1:2 in the presence of a ten-fold molar excess of In placed within alumina crucibles jacketed by fused-silica tubes. The tubes were heated to 1000 °C over 10 h, cooled to 850 °C at a rate of 2 °C h^{-1}, held at this temperature for 2 days, and cooled to 300 °C over 2 days, at which point the liquid indium flux was centrifuged. EDX analyses on these crystals showed the presence of all three elements, and none of the flux elements, in ratios (31–35% *RE*, 7–10% Cr, 60–63% Ge) consistent with the formulas obtained from the structure determinations.

The extent of *RE* substitution was investigated by targeting samples of nominal composition $RECr_{0.3}Ge_2$, prepared by arc-melting mixtures of the elements under an argon atmosphere in an Edmund Bühler MAM-1 compact arc melter. The ingots were placed in evacuated and sealed fused-silica tubes, annealed at 800 °C for 20 days, and then quenched in cold water. $RECr_{0.3}Ge_2$ phases were obtained in essentially quantitative yield for *RE* = Gd–Er, as judged by their powder X-ray diffraction patterns. There was also evidence for the existence of $YbCr_{0.3}Ge_2$ ($a = 4.0917(1)$ Å, $b = 15.5214(5)$ Å, $c = 3.9760(2)$ Å), but the sample contained other phases that could not be identified. The $DyCr_xGe_2$ series was selected to investigate the homogeneity range in Cr, through similar arc-melting and annealing reactions as above.

2.2. Structure determination

Single-crystal X-ray diffraction data for $RECr_xGe_2$ (*RE* = Sm, Gd, Dy) were collected on a Bruker Platform/SMART 1000 CCD diffractometer at 22 °C using ω scans. Structure solution and refinement were carried out with use of the SHELXTL (version 6.12) program package [16]. Face-indexed numerical absorption corrections were applied. Of the possible orthorhombic space groups *Cmcm*, *Cmc*2_1, and *Ama*2 suggested by the systematic absences, the centrosymmetric one *Cmcm* was chosen. Initial atomic positions were located by direct methods, revealing a $CeNiSi_2$-type structure commonly adopted by many REM_xTt_2 phases. Refinements indicated partial occupancy, close to 1/4, of the Cr site. However, the Cr–Ge2 distances (2.1–2.2 Å) are especially short and the Ge2 displacement ellipsoids are unusually oblate within square nets parallel to the *ac* plane. These features are characteristic of REM_xTt_2 phases, where single-crystal structures have been refined [17–19]. Recently, a very weak modulated structure for $TbFe_{0.25}Ge_2$ has been elucidated, based on a four-fold monoclinic supercell in space group $P2_1/n$ [14]. Careful inspection of the intensity frames for $RECr_xGe_2$ did not reveal any obvious additional reflections. Nevertheless, the data frames were re-integrated after cell transformation to the monoclinic superstructure invoked for $TbFe_{0.25}Ge_2$, giving the following cell parameters: $a = 5.8357(8)$ Å, $b = 16.288(2)$ Å, $c = 11.675(1)$ Å, $\beta = 91.865(2)^\circ$ for $SmCr_xGe_2$; $a = 5.800(1)$ Å, $b = 16.128(4)$ Å, $c = 11.636(3)$ Å, $\beta = 91.674(3)^\circ$ for $GdCr_xGe_2$; $a = 5.756(1)$ Å, $b = 15.834(3)$ Å, $c = 11.510(2)$ Å, $\beta = 91.675(3)^\circ$ for $DyCr_xGe_2$. Attempts were made to refine the structures in $P2_1/n$ according to the $TbFe_{0.25}Ge_2$ model, but the reliability factors did not improve and the short Cr–Ge distances remained. These results suggested that $RECr_xGe_2$ likely adopts a different superstructure from $TbFe_{0.25}Ge_2$. In the absence of sufficient evidence in favor of a well-defined superstructure, we present only the average structure ($CeNiSi_2$-type) here.

Powder X-ray diffraction data for all members $RECr_{0.3}Ge_2$ (*RE* = Gd–Er) were refined with the full-profile Rietveld method using the program LHPM-Rietica [20]. Initial positions were taken

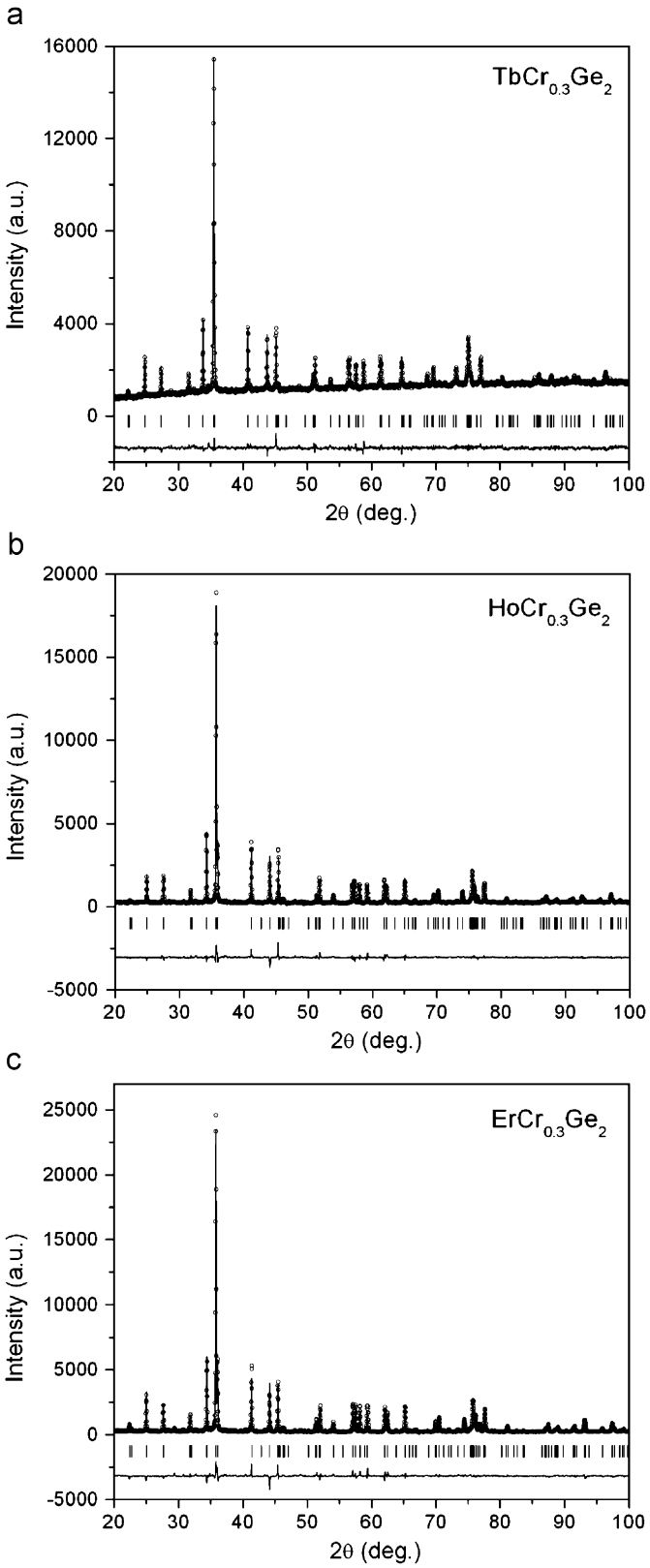

Fig. 1. Rietveld refinement results for $RECr_{0.3}Ge_2$ (*RE* = (a) Tb, (b) Ho, (c) Er). The observed profile is indicated by circles and the calculated profile by the solid line. Bragg peak positions are located by the vertical tic marks. The difference plot is shown at the bottom.

from the single-crystal structures described above. The least-squares refinement included scale factor, background, zero point, cell parameters, pseudo-Voigt peak profile parameters, atomic coordinates, and isotropic displacement parameters. The occupancy of the Cr site was fixed at exactly 0.3, consistent with the initial stoichiometry of the loaded reactants to prepare these phase-pure samples. Only the results for $RECr_{0.3}Ge_2$ (RE = Tb, Ho, Er), where single-crystal data were unavailable, are reported here. Fits to the powder patterns are shown in Fig. 1.

Atomic positions were standardized with the program STRUCTURE TIDY [21]. Crystal data and further details of the data collections are given in Table 1. Final values of the positional and

Table 1
Crystallographic data for $RECr_xGe_2$ (RE = Sm, Gd–Er)

Formula	$SmCr_{0.29(1)}Ge_2$	$GdCr_{0.33(1)}Ge_2$	$TbCr_{0.3}Ge_2$	$DyCr_{0.25(1)}Ge_2$	$HoCr_{0.3}Ge_2$	$ErCr_{0.3}Ge_2$
Formula mass (amu)	*310.66*	319.72	319.71	320.58	325.71	328.04
Space group	*Cmcm* (no. 63)	*Cmcm* (no. 63)	*Cmcm* (no. 63)	*Cmcm* (no. 63)	*Cmcm* (no. 63)	*Cmcm* (no. 63)
a (Å)	4.1939(5)	4.1694(13)	4.1335(3)	4.1303(8)	4.1117(2)	4.1016(2)
b (Å)	16.291(2)	16.136(5)	15.911(1)	15.839(3)	15.7384(8)	15.6579(6)
c (Å)	4.0598(5)	4.0495(13)	4.0107(3)	4.0112(8)	3.9951(2)	3.9876(2)
V (Å^3)	277.38(6)	272.43(15)	263.78(3)	262.42(9)	258.53(2)	256.09(2)
Z	4	4	4	4	4	4
ρ_{calcd} (g cm^{-3})	7.439	7.795	8.047	8.114	8.364	8.504
Technique	Single-crystal XRD	Single-crystal XRD	Powder XRD	Single-crystal XRD	Powder XRD	Powder XRD
Radiation	Mo$K\alpha$	Mo$K\alpha$	Cu$K\alpha_1$	Mo$K\alpha$	Cu$K\alpha_1$	Cu$K\alpha_1$
	λ = 0.71073 Å	λ = 0.71073 Å	λ = 1.54051 Å	λ = 0.71073 Å	λ = 1.54051 Å	λ = 1.54051 Å
μ (mm^{-1})	43.1	46.9	163.0	51.5	89.9	92.9
2θ range	5.0°–60.9°	5.0°–66.1°	20.0°–100.0°	5.1°–66.0°	20.0°–100.0°	20.0°–100.0°
No. of data collected	1617 (R_{int} = 0.037)	1800 (R_{int} = 0.049)	2759 data points	1741 (R_{int} = 0.024)	2759 data points	2759 data points
No. of unique data	264 (256 with $F_o^2 > 2\sigma(F_o^2)$)	321 (294 with $F_o^2 > 2\sigma(F_o^2)$)	90 Bragg reflections	303 (296 with $F_o^2 > 2\sigma(F_o^2)$)	89 Bragg reflections	89 Bragg reflections
No. of variables	19	18	26	19	25	25
Residuals[a]	$R(F)$ = 0.021	$R(F)$ = 0.032	R_B = 0.018	$R(F)$ = 0.022	R_B = 0.046	R_B = 0.060
	$R_w(F^2)$ = 0.056	$R_w(F^2)$ = 0.069	R_p = 0.029	$R_w(F^2)$ = 0.047	R_p = 0.075	R_p = 0.091
			R_{wp} = 0.038		R_{wp} = 0.099	R_{wp} = 0.120

[a] $R_B = \sum |I_o - I_c| / \sum I_o$; $R_p = \sum |y_o - y_c| / \sum y_o$; $R_{wp} = [\sum [w(y_o - y_c)] / \sum w y_o^2]^{1/2}$; $R(F) = \sum ||F_o| - |F_c|| / \sum |F_o|$, (for $F^2 > 2\sigma(F^2)$); $R_w(F_o^2) = [\sum [w(F_o^2 - F_c^2)^2] / \sum w F_o^4]]^{1/2}$, $w^{-1} = [\sigma^2(F_o^2) + (Ap)^2 + Bp]$ where $p = [\max(F_o^2, 0) + 2F_c^2]/3$.

Table 2
Atomic coordinates and equivalent isotropic displacement parameters for $RECr_xGe_2$ (RE = Sm, Gd–Er)[a]

	$SmCr_{0.29(1)}Ge_2$	$GdCr_{0.33(1)}Ge_2$	$TbCr_{0.3}Ge_2$	$DyCr_{0.25(1)}Ge_2$	$HoCr_{0.3}Ge_2$	$ErCr_{0.3}Ge_2$
RE						
y	0.3969(1)	0.3974(1)	0.3965(2)	0.3970(1)	0.3967(1)	0.3969(1)
U_{eq} or U_{iso}	0.0085(2)	0.0076(2)	0.015(1)	0.0099(2)	0.007(1)	0.011(1)
Cr						
occupancy	0.29(1)	0.33(1)	0.3	0.25(1)	0.3	0.3
y	0.1994(3)	0.2004(3)	0.1949(11)	0.1993(3)	0.1961(9)	0.1971(11)
U_{eq} or U_{iso}	0.0067(13)	0.0089(14)	0.009(4)	0.0057(14)	0.013(4)	0.025(5)
Ge1						
y	0.0497(1)	0.0506(1)	0.0510(3)	0.0522(1)	0.0522(2)	0.0527(2)
U_{eq} or U_{iso}	0.0097(2)	0.0093(2)	0.009(2)	0.0120(2)	0.004(1)	0.008(1)
Ge2						
y	0.7518(1)	0.7514(1)	0.7526(3)	0.7519(1)	0.7515(2)	0.7522(2)
U_{eq} or U_{iso}	0.0344(3)	0.0353(4)	0.017(2)	0.0306(3)	0.015(1)	0.015(1)

[a] All atoms are in Wyckoff position 4c (0, y, 1/4). U_{eq} is defined as one-third of the trace of the orthogonalized U_{ij} tensor; U_{iso} applies to results from powder Rietveld refinements.

Table 3
Selected interatomic distances (Å) in $RECr_xGe_2$ (RE = Sm, Gd–Er)

	$SmCr_{0.29(1)}Ge_2$	$GdCr_{0.33(1)}Ge_2$	$TbCr_{0.3}Ge_2$	$DyCr_{0.25(1)}Ge_2$	$HoCr_{0.3}Ge_2$	$ErCr_{0.3}Ge_2$
RE–Ge1 (× 4)	3.046(1)	3.025(1)	2.999(2)	2.989(1)	2.977(1)	2.967(1)
RE–Ge2 (× 2)	3.160(1)	3.141(2)	3.085(3)	3.090(1)	3.070(4)	3.056(1)
RE–Ge2 (× 2)	3.160(1)	3.145(1)	3.106(5)	3.096(1)	3.074(2)	3.070(1)
RE–Ge1 (× 2)	3.255(1)	3.234(1)	3.211(3)	3.210(1)	3.196(2)	3.187(1)
RE–Cr	3.217(5)	3.179(5)	3.21(2)	3.131(5)	3.16(1)	3.128(1)
RE–Cr (× 4)	3.314(2)	3.307(3)	3.226(8)	3.258(2)	3.217(7)	3.217(1)
Cr–Ge2 (× 2)	2.180(2)	2.169(2)	2.173(7)	2.149(2)	2.161(6)	2.146(1)
Cr–Ge2 (× 2)	2.264(2)	2.241(2)	2.262(7)	2.227(2)	2.233(6)	2.225(1)
Cr–Ge1	2.439(5)	2.417(6)	2.29(2)	2.331(5)	2.27(1)	2.262(1)
Ge1–Ge1 (× 2)	2.597(1)	2.601(2)	2.579(5)	2.599(1)	2.586(4)	2.587(1)
Ge2–Ge2 (× 4)	2.919(1)	2.906(1)	2.881(1)	2.879(1)	2.867(1)	2.861(1)

displacement parameters are given in Table 2. Selected interatomic distances are listed in Tables 3. Further data, in CIF format, have been sent to Fachinformationszentrum Karlsruhe, Abt. PROKA, 76344 Eggenstein–Leopoldshafen, Germany, as supplementary material No. CSD-419982 ($SmCr_{0.3}Ge2$), 419986 ($GdCr_{0.3}Ge2$), and 419988 ($DyCr_{0.3}Ge2$), and can be obtained by contacting FIZ (quoting the article details and the corresponding CSD numbers).

2.3. Magnetic measurements

Measurements of dc magnetic susceptibility were made on powders with nominal composition $RECr_{0.3}Ge_2$ (RE = Gd–Er), confirmed to be phase-pure by powder X-ray diffraction, between 2 and 300 K on a Quantum Design 9T–PPMS dc magnetometer/ac susceptometer. The susceptibility was corrected for contributions from the holder and underlying sample diamagnetism. Measurements of ac magnetic susceptibility were made with a driving amplitude of 1–10 Oe and a frequency of 2000 Hz.

3. Results and discussion

3.1. Structure

The germanides REM_xGe_2 were previously known for first-row transition metals being restricted to M = Mn, Fe, Co, Ni, Cu [2], and have now been extended to include an earlier transition metal, M = Cr, in the new series $RECr_xGe_2$. The range of RE substitution is narrower in $RECr_xGe_2$ (RE = Sm, Gd–Er, Yb), and gradually widens on progressing to $REMn_xGe_2$ (RE = Nd, Sm, Gd–Tm, Lu) and REM_xGe_2 (M = Fe, Co, Ni, Cu; RE = Y, La–Sm, Gd–Lu) [12,13]. These compounds adopt the $CeNiSi_2$-type structure, which has been proposed to be more thermodynamically stable than the alternative $YIrGe_2$-type structure adopted by some representatives such as $RENiGe_2$ [22]. Moreover, these $CeNiSi_2$-type phases typically display significant deficiencies on the transition metal site ($0<x<1$), unlike the $YIrGe_2$-type phases which are strictly stoichiometric. The stoichiometric compound $ScCrGe_2$ is also known, but it adopts an unrelated $ZrCrSi_2$-type (or $TiMnSi_2$-type) structure [3,5]. $DyCr_xGe_2$ was chosen as a representative series to investigate the homogeneity range at 800 °C. The cell parameters increase monotonically with greater Cr content in the range $0.25 \leqslant x \leqslant 0.50$, beyond which multiphase products were observed (Fig. 2 and Fig. S1 in Supplementary data). This result conforms to the general trend that x is smaller when M is an early transition-metal (cf., x increases gradually on progressing to a later transition metal, to as high as 1.0 in $RENiGe_2$). Under the nonequilibrium conditions of the flux growth, other competing Cr-containing phases (such as Cr_3Ge and $RECr_6Ge_6$) were also formed, which may account for compositions of the ternary $RECr_xGe_2$ phases not reaching the maximum Cr content observed in arc-melting and annealing reactions.

The structure of $RECr_xGe_2$ consists of $[Cr_xGe_2]$ slabs parallel to the ac plane that are held together by zigzag chains of Ge1 atoms aligned along the c direction, forming a three-dimensional framework with channels occupied by RE atoms (Fig. 3). The Ge–Ge distances within the zigzag chains of Ge1 atoms (~2.6 Å) are shorter and relatively invariant compared to those within the square nets of Ge2 atoms (~2.9 Å) forming part of the $[Cr_xGe_2]$ slabs. Each RE atom is coordinated by 10 Ge atoms, eight at the corners of a square antiprism (four Ge1 and four Ge2) and two Ge1 atoms further away, at distances that gradually decrease with the lanthanide contraction (from 3.046(1)–3.255(1) Å in $SmCr_{0.3}Ge_2$ to 2.967(1)–3.187(1) Å in $ErCr_{0.3}Ge_2$). The Cr atoms are coordinated in square pyramidal geometry, with the distances to the four basal Ge2 atoms being anomalously short (2.146(1)–2.225(1) Å in $ErCr_{0.3}Ge_2$); even the distance to the apical Ge2 atom eventually becomes very short (2.439(5) Å in $SmCr_{0.3}Ge_2$ to 2.262(1) Å in $ErCr_{0.3}Ge_2$), when compared to typical distances of 2.4–2.5 Å in Cr–Ge binaries [23,24] or in $RECrGe_3$ [11], or to the sum of the metallic radii (2.43 Å) [25]. Many defect REM_xGe_2 structures exhibit these anomalously short M–Ge distances, but only in the case of $TbFe_{0.25}Ge_2$ has a modulated superstructure been resolved, in which the square Ge net distorts to form cis–trans chains that can accommodate more reasonable distances to the capping transition-metal atoms [14]. Attempts to detect a superstructure in $RECr_xGe_2$ were unsuccessful, but it is clear that similar distortions of the square Ge net likely take place here.

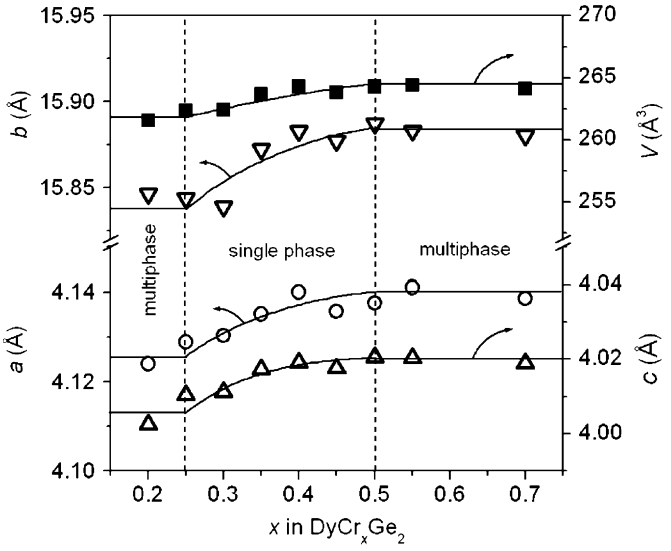

Fig. 2. Plot of cell parameters vs x for $CeNiSi_2$-type phase observed in reactions with nominal composition of $DyCr_xGe_2$.

With the understanding that only the average structure has been determined here, a Zintl–Klemm approach could be applied to draw some simple conclusions about the bonding in $RECr_xGe_2$. If each of the two-bonded Ge1 atoms in the zigzag chains is assigned to be 2– and the Ge2 atoms within the square nets are assumed to be isolated with no involvement in homoatomic bonding, then a charge-balanced stoichiometric formulation "$(RE^{3+})(Cr^{3+})(Ge1^{2-})(Ge2^{4-})$" can be obtained. However, if the experimentally observed Cr deficiency (with $x = \sim 0.3$) is taken into account, then the formulation "$(RE^{3+})(Cr^{3+})_{0.3}(Ge1^{2-})(Ge2^{2-})$" leads to the interesting speculation that the square nets entail weak hypervalent bonding of the Ge2 atoms, similar to that found in many polyantimonides and in accordance with an ideal count of six electrons per atom in a square net [26]. In an alternative bonding picture, the square net acts as an electron donor and the zigzag chain as an electron acceptor in $CeNiSi_2$-type structures [27].

3.2. Magnetic properties

Magnetic data for powder samples of $RECr_{0.3}Ge_2$ (RE = Gd–Er) are shown in Fig. 4 and summarized in Table 4. The zero-field-cooled dc magnetic susceptibility curves measured under low applied magnetic fields (H = 1000 Oe (RE = Gd–Ho) or 5000 Oe (RE = Er)) reveal paramagnetic behavior from 300 K down to relatively low temperatures (below 20 K), at which point

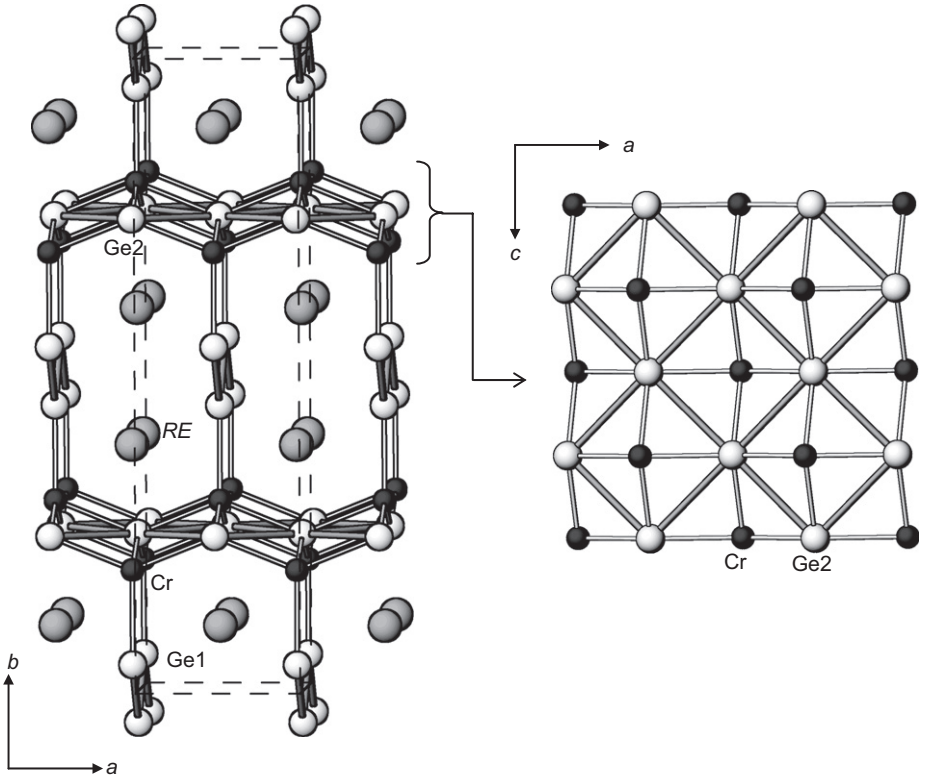

Fig. 3. Average structure of $RECr_xGe_2$ (RE = Sm, Gd–Er) viewed down the c direction and an excised $[Cr_xGe_2]$ slab viewed down the b direction. The large grey spheres are RE atoms, the small solid spheres are Cr atoms, and the medium light spheres are Ge atoms.

downturns in the curves signal the onset of antiferromagnetic ordering. Néel temperatures were located either from plots of $d(\chi T)/dT$ vs T or from ac magnetic susceptibility curves. In the case of the Tb and Dy samples, a second transition at lower temperature is visible in the dc or ac magnetic susceptibility. Magnetic susceptibility measurements on single crystals of $TbFe_{0.25}Ge_2$ also showed two transitions at 2.5 and 19 K when the external magnetic field was applied parallel and perpendicular to the crystallographic b-axis, respectively [14]. These transitions were attributed to the Tb atoms experiencing a strong anisotropy between the interslab and intraslab magnetic interactions, as discussed below, and an analogous mechanism is likely operative in the isostructural $TbCr_{0.3}Ge_2$ and $DyCr_{0.3}Ge_2$ compounds here. In the case of the Er sample, a transition is seen at 2 K in the ac susceptibility but not the dc susceptibility curve. At first glance, this may be attributable to trace amounts of ferrimagnetic $ErCr_6Ge_6$ impurities [10] found in this sample, but the saturation magnetization of 8 μ_B at 2 K is substantial (cf., theoretical value of 9.0 μ_B for Er^{3+}) and there is a divergence in the field-cooled vs. zero-field-cooled curves. This behavior is similar to that seen in $ErCo_{0.47}Ge_2$ and $ErCu_{0.25}Ge_2$, whose detailed magnetic structures have been determined [28,29].

In the high-temperature paramagnetic regime, the linear portion of the inverse magnetic susceptibility was fit to the Curie-Weiss law, $\chi = C/(T-\theta_p)$. The Weiss parameters θ_p are small and negative for RE = Gd, Tb, and Ho, implying antiferromagnetic coupling, but they are small and positive for RE = Dy and Er, implying ferromagnetic coupling. These trends are observed in related REM_xGe_2 compounds [14,15,28–41]. The effective magnetic moments determined from the Curie constants C are close to or slightly greater than the theoretical free-ion values for RE^{3+}. Thus, essentially all the magnetism originates from the magnetic moments of f electrons localized on the RE atoms. The d electrons on the Cr atoms provide little or no contribution and are presumably delocalized, but this would need to be confirmed by band structure calculations or resistivity measurements. The isothermal magnetization curves at 2 K, below the Néel temperature, reveal an increasing tendency towards saturation behavior on proceeding from RE = Gd to Er, and suggest the occurrence of metamagnetism in the case of RE = Tb, Dy, and Ho. The Dy and Ho samples display a slight hysteresis that is manifested only at intermediate fields (between 20 and 60 kOe) and vanishes as the applied field returns to zero.

Magnetic susceptibilities for different Cr contents (x = 0.25, 0.35, 0.45) in the $DyCr_xGe_2$ series have also been measured (Fig. 5). Surprisingly, the transition at 12 K is little changed and the lower-temperature transition only tends to become slightly less prominent with greater Cr content. This relatively insensitivity may be attributed to the small change in unit cell parameters (~0.3% in the cell lengths and ~0.8% in cell volume) within the homogeneity range of $DyCr_xGe_2$ (Fig. 2). In contrast, a neutron diffraction study of the $TbNi_xGe_2$ (x = 0.6–1.0) series indicated a strong dependence with T_N increasing from 31 to 42 K with greater Ni content [34].

These results are generally consistent with the magnetic data previously reported for other REM_xGe_2 (M = Mn, Fe, Co, Ni, Cu) compounds with the $CeNiSi_2$-type structure [14,15,28–41]. Most of these compounds are antiferromagnetic at similarly low temperatures (notable exceptions are $PrNiGe_2$ and $NdNiGe_2$, which are ferromagnetic) and exhibit effective magnetic moments close to the free-ion RE^{3+} values (except for the Mn-containing compounds, where local Mn moments are observed) [15]. The diverse magnetic behavior originates from the competition of interactions possible between the RE atoms, which are arranged in double-layer slabs stacked along b (Fig. 3). The RE–RE distances within these slabs are close to ~4.0 Å, whereas those between the slabs are ~5.6 Å. The RE moments cannot interact directly with each other because they are too far apart, but they can couple

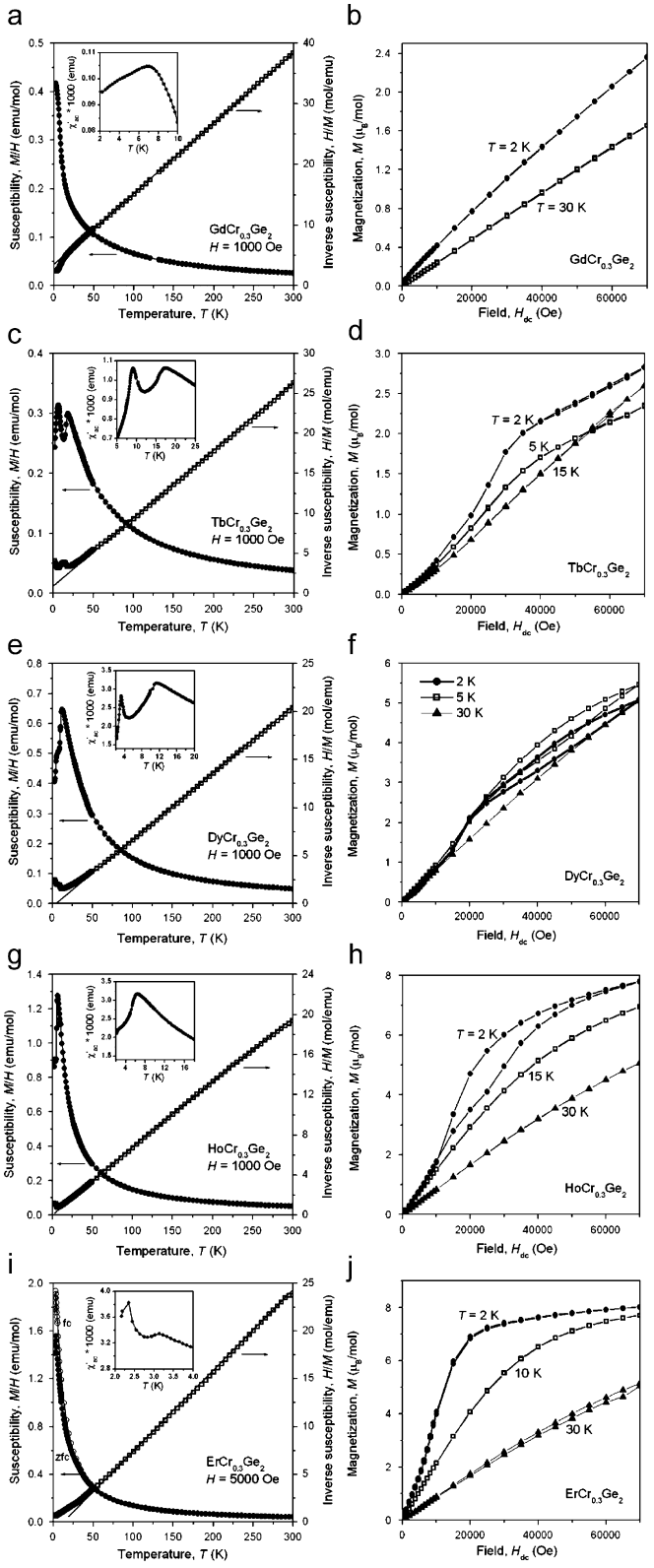

Fig. 4. Magnetic data for $RECr_{0.3}Ge_2$ (RE = Gd–Er). The left panels show the zero-field-cooled dc magnetic susceptibility and its inverse as a function of temperature (with the insets highlighting low-temperature transitions in the ac magnetic susceptibility), and the right panels show isothermal magnetization curves at various temperatures. The field-cooled susceptibility is also shown in the case of $ErCr_{0.3}Ge_2$.

Table 4
Summary of magnetic data for $RECr_{0.3}Ge_2$ (RE = Gd–Er)

	$GdCr_{0.3}Ge_2$	$TbCr_{0.3}Ge_2$	$DyCr_{0.3}Ge_2$	$HoCr_{0.3}Ge_2$	$ErCr_{0.3}Ge_2$
T_N (K) from:					
$d(\chi T)/dT$ vs T plot	10.2	4.3, 16.1	4.0, 9.9	5.5	2.5
χ'_{ac} vs T plot	7.0	9.1, 17.4	3.2, 11.2	6.4	3.1
θ_p (K)	−28.4(2)	−9.9(2)	4.5(2)	−2.3(2)	16.6(3)
$\mu_{eff,\ meas}$ (μ_B/f.u.)	8.26(1)	9.73(1)	10.76(1)	11.08(1)	9.67(1)
$\mu_{eff,\ theor}$ for RE^{3+} (μ_B)	7.94	9.72	10.65	10.61	9.58

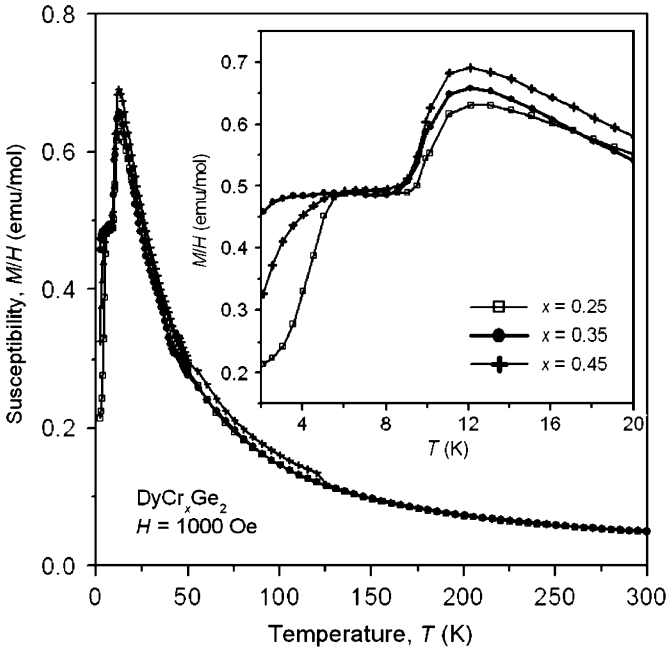

Fig. 5. Zero-field-cooled dc magnetic susceptibility for several members of $DyCr_xGe_2$ ($x = 0.25,\ 0.35,\ 0.45$). The inset highlights the low-temperature transitions.

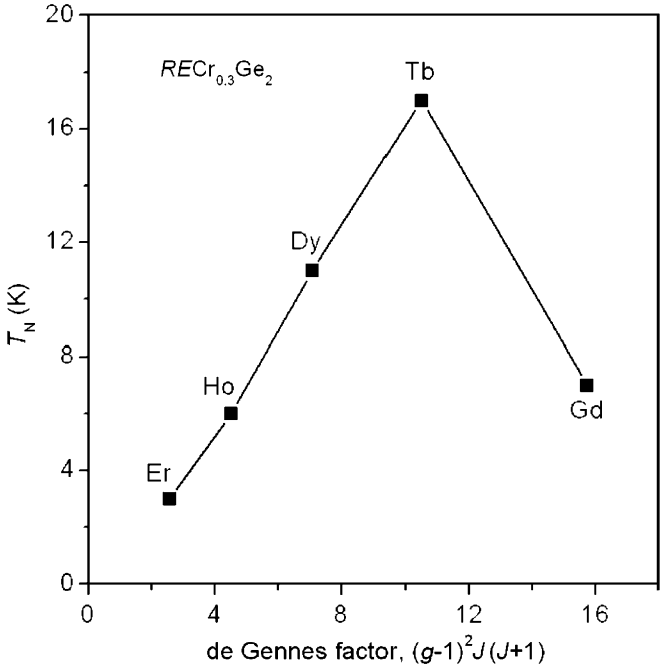

Fig. 6. Magnetic ordering temperatures for $RECr_{0.3}Ge_2$ plotted vs the de Gennes factor.

indirectly through spin polarization of conduction electrons (RKKY model). Support for this mechanism in $RECr_xGe_2$ comes from the observation that T_N scales with the de Gennes factor (Fig. 6). The deviation found for the Gd member is typically seen in other REM_xGe_2 series and normally attributed to contributions from crystalline electric field (CEF) effects. In most REM_xGe_2 compounds, the magnetic moments are coupled ferromagnetically within the slabs (parallel to the *ac* plane) and antiferromagnetically between them (along the *b* direction). Within this highly anisotropic arrangement of *RE* atoms, a variety of complex magnetic structures are possible depending on the relative strengths of these coupling interactions. Although the Cr atoms do not contribute to the total magnetic moment, the delocalized 3*d* electrons play an important role as the intermediary between the 4*f* moment coupling of the *RE* atoms.

The prevalent REM_xGe_2 phases with the $CeNiSi_2$-type structure have been extended to the earliest transition-metal representative thus far in $RECr_xGe_2$. We have attempted to prepare the corresponding silicides, $RECr_xSi_2$, but to no avail. In recognition that only the average structure has been determined, as signaled by anomalously short Cr–Ge distances, it will be important to seek evidence for a superstructure through other methods such as electron diffraction. Analyses of the pair distribution function, obtained from synchrotron data, are in progress to understand the local structure around the Cr atoms. These compounds undergo antiferromagnetic ordering at low temperatures, with complex magnetic structures that will need to be elucidated in more detail by neutron diffraction studies.

Acknowledgments

The Natural Sciences and Engineering Research Council of Canada and the University of Alberta supported this work. We thank Dr. Robert McDonald and Dr. Michael J. Ferguson (X-ray Crystallography Laboratory) for the X-ray data collection and Ms. Christina Barker (Department of Chemical and Materials Engineering) for assistance with the EDX analysis.

Appendix A. Supporting Information

Supplementary data associated with this article can be found in the online version at doi:10.1016/j.jssc.2008.10.013.

References

[1] P.S. Salamakha, O.L. Sologub, O.I. Bodak, in: K.A. Gschneidner Jr., L. Eyring (Eds.), Handbook on the Physics and Chemistry of Rare Earths, vol. 27, Elsevier, Amsterdam, 1999, pp. 1–223.
[2] P.S. Salamakha, in: K.A. Gschneidner Jr., L. Eyring (Eds.), Handbook on the Physics and Chemistry of Rare Earths, vol. 27, Elsevier, Amsterdam, 1999, pp. 225–338.
[3] B.Ya. Kotur, A.B. Kravs, R.I. Andrusyak, Russ. Metall. (6) (1988) 192–195 (Transl. Izv. Akad. Nauk SSSR, Metally (6) (1988) 198–201).
[4] B.Ya. Kotur, R.I. Andrusyak, V.E. Zavodnik, Sov. Phys. Crystallogr. 33 (1988) 141–142 (Transl. Kristallografiya 33 (1988) 240–241).
[5] G. Venturini, M. Meot-Meyer, B. Roques, J. Less-Common Met. 107 (1985) L5–L7.
[6] A.M. Guloy, J.D. Corbett, Inorg. Chem. 32 (1993) 3532–3540.
[7] O.I. Bodak, E.I. Gladyshevskii, P.S. Salamakha, V.K. Pecharskii, V.A. Bruskov, Sov. Phys. Crystallogr. 34 (1989) 774–775 (Transl. Kristallografiya 34 (1989) 1285–1287).
[8] A.V. Morozkin, Yu.D. Seropegin, V.K. Portnoy, I.A. Sviridov, A.V. Leonov, Mater. Res. Bull. 33 (1998) 903–908.
[9] J.H.V.J. Brabers, K.H.J. Buschow, F.R. de Boer, J. Alloys Compd. 205 (1994) 77–80.
[10] P. Schobinger-Papamantellos, J. Rodríguez-Carvajal, K.H.J. Buschow, J. Alloys Compd. 256 (1997) 92–96.
[11] H. Bie, O. Ya. Zelinska, A.V. Tkachuk, A. Mar, Chem. Mater. 19 (2007) 4613–4620.
[12] M. François, G. Venturini, B. Malaman, B. Roques, J. Less-Common Met. 160 (1990) 197–213.
[13] G. Venturini, M. François, B. Malaman, B. Roques, J. Less-Common Met. 160 (1990) 215–228.
[14] M.A. Zhuravleva, D. Bilc, R.J. Pcionek, S.D. Mahanti, M.G. Kanatzidis, Inorg. Chem. 44 (2005) 2177–2188.
[15] A. Szytuła, J. Leciejewicz, Handbook of Crystal Structures and Magnetic Properties of Rare Earth Intermetallics, CRC Press, Boca Raton, FL, 1994.
[16] G.M. Sheldrick, SHELXTL, Version 6.12, Bruker AXS Inc., Madison, WI, 2001.
[17] L. Zeng, H.F. Franzen, J. Alloys Compd. 267 (1998) 86–89.
[18] L. Paccard, D. Paccard, J. Allemand, J. Less-Common Met. 161 (1990) 295–298.
[19] J. Kończyk, P. Demchenko, R. Matvijishyn, V. Pavlyuk, B. Marciniak, Acta Crystallogr. Sect. E 62 (2006) i4–i6.
[20] B. Hunter, LHPM-Rietica, Version 1.7.7, International Union of Crystallography Commission on Powder Diffraction Newsletter, no. 20 (summer), 1998 〈www.rietica.org〉.
[21] L.M. Gelato, E. Parthé, J. Appl. Crystallogr. 20 (1987) 139–143.
[22] J.R. Salvador, J.R. Gour, D. Bilc, S.D. Mahanti, M.G. Kanatzidis, Inorg. Chem. 43 (2004) 1403–1410.
[23] P. Israiloff, H. Völlenkle, A. Wittmann, Monatsh. Chem. 105 (1974) 1387–1404.
[24] H. Völlenkle, A. Preisinger, H. Nowotny, A. Wittmann, Z. Kristallogr. 124 (1967) 9–25.
[25] L. Pauling, The Nature of the Chemical Bond, 3rd ed, Cornell University Press, Ithaca, NY, 1960.
[26] G.A. Papoian, R. Hoffmann, Angew. Chem. Int. Ed. 39 (2000) 2408–2448.
[27] D.M. Proserpio, G. Chacon, C. Zheng, Chem. Mater. 10 (1998) 1286–1290.
[28] S. Baran, F. Henkel, D. Kaczorowski, J. Hernandez-Velasco, B. Penc, N. Stüsser, A. Szytuła, E. Wawrzyńska, J. Alloys Compd. 415 (2006) 1–7.
[29] A. Gil, D. Kaczorowski, J. Hernandez-Velasco, B. Penc, E. Wawrzyńska, A. Szytuła, J. Alloys Compd. 384 (2004) L4–L6.
[30] I. Das, E.V. Sampathkumaran, Solid State Commun. 83 (1992) 765–770.
[31] A. Gil, J. Leciejewicz, K. Małetka, A. Szytuła, Z. Tomkowicz, K. Wojciechowski, J. Magn. Magn. Mater. 129 (1994) L155–L159.
[32] V. Ivanov, L. Vinokurova, A. Szytuła, J. Alloys Compd. 218 (1995) L24–L27.
[33] V. Ivanov, A. Szytuła, J. Alloys Compd. 252 (1997) L22–L25.
[34] P. Schobinger-Papamantellos, K.H.J. Buschow, C. Ritter, J. Alloys Compd. 287 (1999) 51–56.
[35] A. Gil, K. Tubielewicz, Metallofiz. Noveishie Tekhnol. 23 (2001) 153–165.
[36] A. Gil, M. Hofmann, B. Penc, A. Szytuła, J. Alloys Compd. 320 (2001) 29–32.
[37] A.P. Pikul, D. Kaczorowski, Z. Bukowski, T. Plackowski, K. Gofryk, J. Phys. Condens. Matter 16 (2004) 6119–6128.
[38] A. Gil, B. Penc, J. Hernandez-Velasco, E. Wawrzyńska, A. Szytuła, J. Alloys Compd. 387 (2005) L8–L10.
[39] S. Baran, Ł. Gondek, J. Hernandez-Velasco, D. Kaczorowski, A. Szytuła, J. Magn. Magn. Mater. 285 (2005) 188–192.
[40] A. Gil, Mater. Sci.—Poland 24 (2006) 577–583.
[41] A. Szytuła, B. Penc, D. Kaczorowski, A. Arulraj, S. Baran, N. Stüsser, K. Tomala, J. Alloys Compd. 460 (2008) 120–124.